Copyright © 2012 Tech Science Press CMES, vol.86, no.3, pp.225-240, 2012

Modeling and Simulation of Phantom Temperature Field in Magnetic Induction Hyperthermia

J.H. Wu[1], L.Y. Zhu[2] and J.T. Tang[3]

Abstract: Magnetic induction hyperthermia is one of hopeful methods for tumor therapy. In this method, several ferromagnetic seeds are needed to be implanted into the tumor. The seeds would produce energy, and cause the nearby tumor to die. Temperature prediction is significant before treatment. In addition, in clinical treatment, the tumor temperature has to be monitored in realtime. However, using as few thermometers as possible is the basic principle. Fortunately, the numerical simulation can contribute to realtime measurement. The seed temperature is modeled based on the Haider's method, which is treated as the thermal boundary in numerical simulation. We employ the lattice Boltzmann method to solve the bioheat transfer equation. Meanwhile, three phantom experiments are carried out to evaluate the model. Thirty-two thermal seeds in total were implanted into a phantom, and three thermocouples are embedded into the specific positions to record the variation of temperature. By comparing the results of simulations and experiments, we obtain that the proposed numerical model is effective.

Keywords: Magnetic induction hyperthermia, Temperature modeling, Lattice Boltzmann method, Ferromagnetic seed.

1 Introduction

Magnetic induction hyperthermia for tumor has been developed for many years(Murray, Steeves, Gentry, Bresnick, Boldt, Mieler, and Tompkins (1997); Steeves, Murray, Moros, Boldt, Mieler, and Paliwal (1992); Brezovich, Lilly, Meredith, Weppelmann, Henderson, Brawner, and Salter (1990)). In ferromagnetic interstitial hyperthermia, a number of ferromagnetic seeds are required to be implanted into the tumor according to its shape. The seeds can produce energy under an alternating

[1] Key Laboratory of Particle & Radiation Imaging (Tsinghua University), Ministry of Education, Beijing, CHINA
[2] Fuzhou Haolian Medical Technology Co., Ltd., Beijing, CHINA
[3] Department of Engineering Physics, Tsinghua University, Beijing, CHINA

magnetic field. As soon as the alternating magnetic field is exerted, the seeds would be heated. Then, the temperature of the tumor would rise due to the energy transfer from the seeds(Tompkins, Partington, Steeves, Bartholow, and Paliwal (1992)). Once the temperature reaches to a critical value(normally $43^{\circ}C$), the tumor cells would lose activity. After a period of therapy, the tumor will die. When the temperature of the seed approaches to its Curie point, it would not absorb energy again. Then the temperature of the seed will maintain until the magnetic field is lost. Owing to this property, the temperature of the normal tissue would stay at a safe level. Therefore, the magnetic induction hyperthermia is safe.

Treatment planning system(TPS) can be used to predict the temperature distribution in the tumor before the clinical treatment(Kotte, Wieringen, and Lagendijk (1998)). The heat conduction model and the effective solving method determine the reliability of TPS. Typical heat conduction model for the human body is the Pennes bioheat transfer equation(Pennes (1948)), which was often solved by the finite volume method(Indik, Indik, and Cetas (1994)). However, when the number of grids are large, it would cost too much calculation time. As a time and space discrete method, lattice Boltzmann method(LBM)(Chen and Doolen (1998)) is very suitable for parallel computing. He, Chen, and Doolen (1998) developed a LBE for the thermal problems. Golneshan and Lahonian (2011) have given an example of obtaining the temperature distribution in spherical tissue with LBM. Another important factor influencing temperature distribution is the model of the ferromagnetic seed. We treat the seed as the thermal boundary and develop a temperature discrete model based on Haider's experimental model(Haider, Cetas, Wait, and Chen (1991)) .

We present a model to predict the temperature field for tumor in magnetic induction hyperthermia. The solution of the Pennes heat transfer equation by LBM are described. The boundary treatment methods are suggested. We carried out three identical phantom experiments. Each muscle phantom contained with 32 ferromagnetic seeds. We record the temperature variations with three thermal electric couples. Meanwhile, the numerical simulations with the proposed LBM are implemented. The comparing results show the proposed method has enough accuracy for treatment planning before the clinical therapy.

2 Numerical Method

2.1 Pennes bioheat transfer equation

In this study, we employ the pennes bioheat equation to model the temperature distribution in human body.

$$k\nabla^2 T + \eta_b \rho_b c_{pb}(T_a - T) + Q_m + Q_s = \rho c_p \frac{\partial T}{\partial t} \tag{1}$$

where ρ is the density, c_p is the specific heat, k is the thermal conductivity of the tissue, T is the temperature, T_a is the temperature of the artery, t is the time, ρ_b, c_{pb} are the density and the specific heat of the blood, η_b and Q_m are the blood perfusion and the metabolic heat generation of the tissue, Q_s is the distributed volumetric heat source due to spatial heating.

Eq. (1) can be rewritten as:

$$k\nabla^2 T + Q = \rho c_p \frac{\partial T}{\partial t} \tag{2}$$

where Q contains all the heat source by the body tissue, which is

$$Q = \eta_b \rho_b c_{pb}(T_a - T) + Q_m + Q_s \tag{3}$$

2.2 Lattice Boltzmann method for heat conduction

After the simple transformation mentioned above, the bioheat transfer equation becomes an ordinary transient heat transfer equation. The transient heat transfer equation could be solved by LBM.

Typical lattice Boltzmann equation for heat transfer is defined as:

$$g_i(\mathbf{x} + \mathbf{e}_i\delta_t, t + \delta_t) - g_i(\mathbf{x}, t) = -\frac{1}{\tau}[g_i(\mathbf{x}, t) - g_i^{eq}(\mathbf{x}, t)] + \delta_t F_i \tag{4}$$

where $g_i(\mathbf{x}, t)$ is the distribution function, i is the direction, $g_i^{eq}(\mathbf{x}, t)$ is the equilibrium distribution function, $\mathbf{x}$ is the grid position, $\mathbf{x} + \mathbf{e}_i\delta_t$ is the neighbor of $\mathbf{x}$ in the direction of i, $\mathbf{e}$ is the velocity that the distribution moves from the site $\mathbf{x}$ to the neighboring site $\mathbf{x} + \mathbf{e}_i\delta_t$, τ is the relaxation parameter, F_i is the distribution function of the source term .

Different from what He, Chen, and Doolen (1998) had suggested, we prefer another simpler form of the source term

$$F_i(\mathbf{x}, t) = \omega_i Q(\mathbf{x}, t) \tag{5}$$

The equilibrium distribution functions are defined as:

$$g_i^{eq}(\mathbf{x},t) = \omega_i T \tag{6}$$

Then, the macro temperature variable is defined as:

$$T = \sum_{i=0}^{q-1} g_i(\mathbf{x},t) \tag{7}$$

where q is the total amounts of the lattice vectors.

In this paper, we adopt a D3Q19 model, showed in Fig. 1. The lattice velocity $\mathbf{e}$ is defined as:

$$\begin{bmatrix} 0 & 0 & 0 & 1 & -1 & 0 & 0 & 1 & -1 & 1 & -1 & 0 & 0 & 0 & 0 & 1 \\ 0 & 1 & -1 & 0 & 0 & 0 & 0 & 1 & 1 & -1 & -1 & 1 & 1 & -1 & -1 & 0 \\ 0 & 0 & 0 & 0 & 0 & 1 & -1 & 0 & 0 & 0 & 0 & 1 & -1 & 1 & -1 & 1 \end{bmatrix}$$
$$\begin{bmatrix} 1 & -1 & -1 \\ 0 & 0 & 0 \\ -1 & 1 & -1 \end{bmatrix} \tag{8}$$

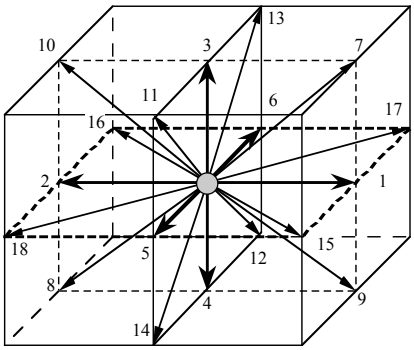

Figure 1: D3Q19 velocity model

The weight factor w_i is give by

$$w_i = \begin{cases} 1/3, & i = 0 \\ 1/18, & i = 1,2,\cdots,6, \\ 1/36, & i = 7,8,\cdots,18 \end{cases} \tag{9}$$

Here, we adopt a central difference method for the term $F_i(\mathbf{x},t)$,

$$F_i(\mathbf{x},t) = \omega_i Q(\mathbf{x} + \frac{\mathbf{e}_i \delta_t}{2}, t + \frac{\delta_t}{2}) \tag{10}$$

Hence, Eq. (10) can derive the macro temperature without any other modification. By applying Taylor expansion, Eq. (10) is rewritten as:

$$F_i(\mathbf{x},t) = \omega_i Q(\mathbf{x},t) + \frac{\delta_t}{2}(\partial_t + \mathbf{e}_i \nabla) Q(\mathbf{x},t) \tag{11}$$

By Chapmann-Enskog multiscale expansion, Eq. (4) can be reduced to the macro heat conduction equation as displayed in Eq. (1), as long as the relaxation parameter and the thermal diffusivity satisfy the relation as below:

$$\tau = 0.5 + \frac{a\delta_t}{\xi \delta_x^2} \tag{12}$$

where $a = \frac{k}{\rho c_p}$ is the thermal diffusivity, ξ is a coefficient, which is correlated with the model and the wight factor, in the current case, $\xi = 3$.

2.3 Solution of LB

The procedure of LB solution contains two steps, i.e. the collision step and the streaming step. In streaming process, the distribution functions move to the neighboring sites in their respective directions.

$$g_i^{'}(\mathbf{x},t) = g_i(\mathbf{x} - \mathbf{e}_i \delta_t, t) \tag{13}$$

Before the collision step, the macro variables is required to be calculated with Eq. (7),

$$T = \sum_{i=0}^{q-1} g_i^{'}(\mathbf{x},t) \tag{14}$$

At the collision steps, all the incoming distribution functions $g_i^{'}(\mathbf{x},t)$ collide with the particles, which stayed at the original site. Then, the new distribution function is formed:

$$g_i(\mathbf{x}, t+\delta_t) = (1 - \frac{1}{\tau}) g_i^{'}(\mathbf{x},t) + \frac{1}{\tau} g_i^{eq}(\mathbf{x},t) \tag{15}$$

where $g_i^{eq}(\mathbf{x},t)$ is obtained from a predefined equilibrium function, at present study, the function is

$$g_i^{eq}(\mathbf{x},t) = \omega_i T \tag{16}$$

where, ω_i is the coefficient, the value can be defined by several simple formulas.

2.4 Boundary conditions

Boundary conditions are significant in numerical simulation. Improper boundary conditions would produce great mistakes. Guo, Zheng, and Shi (2002) and Latt, Chopard, Malaspinas, Deville, and Michler (2008) have summarized and recommended many boundary treatments. In this work, non-equilibrium extrapolation method developed by Guo, Zheng, and Shi (2002) is employed.

The main method is to substitute the nonequilibrium distribution of the boundary node with its neighboring grids. If the grid $\mathbf{x}$ is the boundary grid, $\mathbf{x}_{nb}$ is the nearest neighbor grid, then, the distribution of the grid $\mathbf{x}$ is given by

$$g_i(\mathbf{x}) = g_i^{eq}(\mathbf{x}) + g_i(\mathbf{x}_{nb}) - g_i^{eq}(\mathbf{x}_{nb}) \tag{17}$$

Non-equilibrium extrapolation method has high accuracy, which is almost suitable for all the boundary conditions.

3 Temperature model of the ferromagnetic seeds

In this case, the heat sources in body tissue are the ferromagnetic seeds, which have been implanted into the tumor. The seeds would produce heat under the alternating magnetic field. It is the magnetic eddy current effect. The seeds become paramagnetic after the temperature of the seeds reach to the curie point. Then, the temperature remain unchanged, as well known, which is the Curie point phenomenon. Nevertheless, when the temperature drops lower than the curie point, they would absorb the energy again. We note this is a nonlinear process.

3.1 The experimental model of the seed

As the temperature variation of the seed is complicated, it is no necessary to be calculated by the numerical methods. In this study, the seeds are treated as the heat boundary. We use the Haider's experimental equation(Haider, Cetas, Wait, and Chen (1991)) to describe the power absorbed by the seeds, therefore, the temperature of the seeds can be determined. The absorption power is given by:

$$P(T) = \frac{P_0}{1 + e^{\beta(T - T_e) + 2}} \tag{18}$$

where $P(T)$ is the absorption power of the ferromagnetic rod per unit length, T_c is the curie temperature, $\beta/4$ represents the gradient of curve close to the curie temperature. P_0 can be written as(Stauffer, Cetas, and Jones (1984); Stauffer, Cetas, Fletcher, Deyoung, Dewhirst, Oleson, and Roemer (1984))

$$P_0 = \pi r_a (\omega \mu_{max}/2\sigma)^{\frac{1}{2}} H_0^2 \tag{19}$$

where μ_{max} is the maximum magnetic conductivity($H \cdot m_{-1}$), σ is the conductivity($S \cdot m_{-1}$), ω is the frequency of the magnetic field, r_a is the radius of ferromagnetic rod(m), H_0 is the magnetic field intensity($A \cdot m_{-1}$).

The ratio of the power absorption to the maximum power absorption is represented by $p = \frac{P(T)}{P_0}$, which is a function of temperature T, the relationship of the seed between p and T used in the experiment is illustrated in Fig. 2.

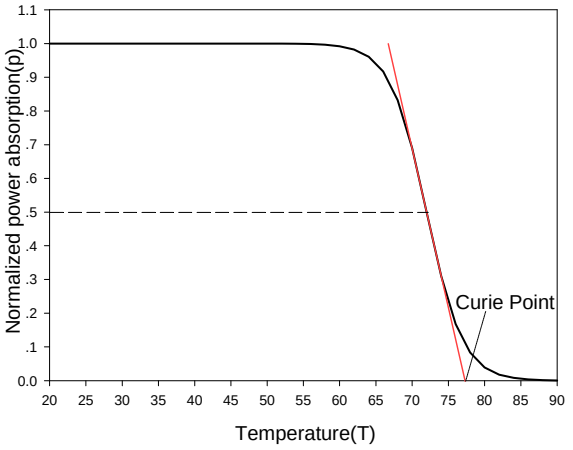

Figure 2: The ratio of power absorption respect to the temperature

We can see from Fig. 2, that the Curie temperature of the seed, that have been utilized in the experiments, is $77°C$. Once the temperature of the seed is beyond the Curie point, the absorbed energy is almost close to zero.

3.2 The numerical model of the seed

The energy exchange between the seed and the phantom is very complicated. This study does not use numerical methods to analyze the internal thermal variation of the seed, which would obviously increase the difficulty of calculation. We treat the seeds as the thermal boundaries. Therefore, as long as the temperature of the seed is known, the simulation will proceed.

In simulation, the time increment is denoted as δt, and the current temperature of

the seeds is T, then, the absorbed energy during a time step δt is

$$E(T) = \begin{cases} P\delta t & T < T_c \\ 0 & T \geq T_c \end{cases} \tag{20}$$

According to the heat conduction equation, the temperature increment is

$$\delta T = \frac{E(T)}{c_p \rho \pi r^2} \tag{21}$$

where, $c_p(Jkg^{-1}K^{-1})$ is the specific heat of the seeds, ρ is the seed density, r is the radius of the seed.

Now, the temperature at time $t + \delta t$ is

$$T(t + \delta t) = \delta T + T(t) \tag{22}$$

If the ferromagnetic seeds are placed in the vacuum magnetic field, the temperature would increase to the Curie point in a short time, and keep until the magnetic field is vanished. This process is illustrated in Fig. 3. The initial temperature is assumed as $26°C$, the temperature will reach to the Curie point in 5 seconds. However, the actual temperature variation is not the same as what displayed in Fig. 3. As there have energy transfer between the seed and the mediums, actual heating would be slower.

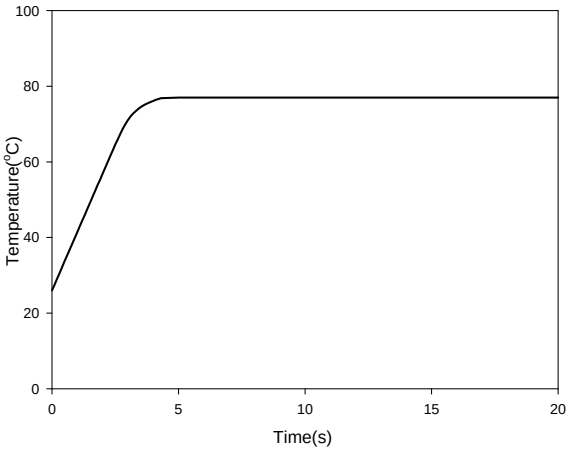

Figure 3: Temperature variation of the ferromagnetic seed

4 Results and Discussion

4.1 Experiment of the magnetic induction heat on phantom

The experiment of using magnetic induction to heat up the phantom is introduced. The magnetic field is generated by a magnetic induction hyperthermia device, which is located in our laboratory, as shown in Fig. 4(a). The seed we utilized is a $0.8mm$ diameter and $6mm$ long Ni-Cu alloy(Fig. 4(b)), which has perfect super paramagnetic. The device and the seeds are all produced by Fuzhou Haolian Medical Technology Co., Ltd. The curie point of the seed is about $76°C$. The other parameters are listed in Table 1.

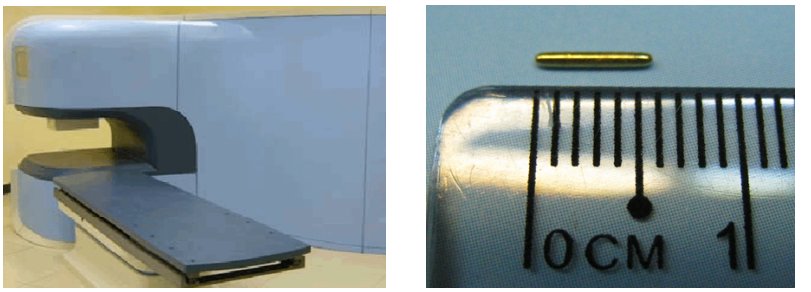

(a) Magnetic field generator (b) Ferromagnetic seeds

Figure 4: Experimental devices

Table 1: The values of some parameters

Name	Symbol	Value
Curie temperature	$T_c(°C)$	77
Gradient of curve	β	0.4
Maximum magnetic permeability	$\mu_{max}\ (H \cdot m_{-1})$	1.885×10^{-4}
Thermal conductivity of the seed	$k_s\ (Wm^{-1}K^{-1})$	22
The electric conductivity of the seed	$\sigma(S \cdot m_{-1})$	2×10^6
Frequency of alternating magnetic field	ω(kHz)	$2\pi \times 110$
Radius of the seed	$r_a(m)$	0.4×10^{-3}
Magnetic field intensity	$H_0(A \cdot m_{-1})$	2000
Density of the phantom	$\rho\ (kgm^{-3})$	1050
Specific heat	$c_p\ (Jkg^{-1}K^{-1})$	3800
Thermal conductivity of the phantom	$k\ (Wm^{-1}K^{-1})$	0.27
Local metabolism	$Q_m\ (W/m^3)$	0

The phantom used in the experiment is a $60mm \times 60mm \times 60mm$ cube, with 32 ferromagnetic seeds have been implanted. These seeds are divided into two groups, which formed two parallel layers, each layer contains 16 seeds, as displayed in Fig. 5, the solid circles represent the seeds, the spacing between the two seeds is $10mm$, they form a 4×4 matrix.

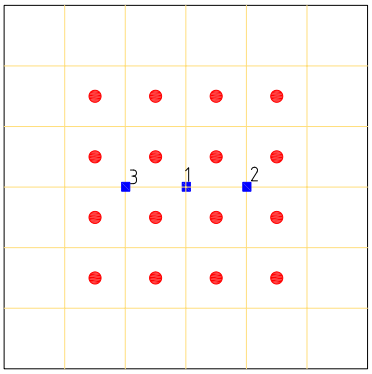

Figure 5: Schematic of the distribution of the seeds

At the central plane of the two seed layers, three thermocouples are embedded, which are marked as the solid squares in Fig. 6. The second and third thermocouples are symmetrically placed. The purpose is to decrease the measurement error, as the thermocouple would be placed to the wrong places.

The phantom, which contains the seeds, is placed between the two magnetic poles. Once the device started, the alternating magnetic field is produced, the temperature of the seeds will increase, then, the phantom is heated. In the meantime, the thermometer will record the temperature values at any time.

The same as the seeds, the thermocouples are implanted into the phantom by the puncture needle with a module plate. Nevertheless, the couples are difficult to be place to the exact positions. Therefore, three identical experiments were carried out. The initial and the final temperatures of the phantom are listed in Table. 2

4.2 Comparison between simulations and experiments

As described before, several LB models can be applied, such as D3Q7, D3Q15 and D3Q19. The model of D3Q19 is employed in this simulation. The wight factors illustrated in Eq. (9), in this case, ξ is $\frac{1}{3}$. The unit length of each cell is $\delta_x = 1$, the number of the grid in x, y, z direction are 60 respectively. As the phantom has no internal source, the relaxation parameter can be defined arbitrarily, we choose that $\delta_t = 1$, then, the relaxation parameter is determined.

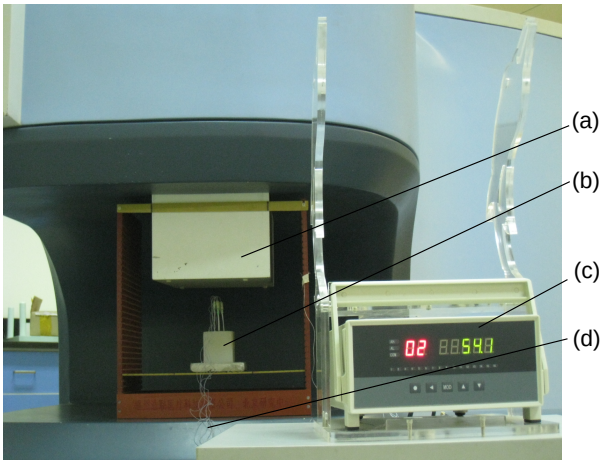

Figure 6: Schematic of the experiment (a)Magnetic pole, (b)Phantom, (c)Thermometer, (d)Thermocouple

Table 2: The results obtained from the experiment

Phantom number	Point $1(^{\circ}C)$	Point $2/3(^{\circ}C)$	Initial temperature$(^{\circ}C)$	Environmental temperature$(^{\circ}C)$
1	61.7	59.25	19.23	22.5
2	62.2	59.9	20.17	23.9
3	61.5	59.3	20.07	23.7
Average	61.8	59.5	19.82	23.37

The diameter of the ferromagnetic seed is $0.8mm$. We define the grid size as $1mm$, therefore, 6 grids can represent one ferromagnetic seed. The heat source is also dealt as the boundary. If the lost energy that has transferred into the phantom is ignored, the temperature at any time step, can be obtained from Eq. (22). Although, the lost energy is very little, we present a simple solving method,

$$T^{'}(t+\delta t) = T(t+\delta t) - T_{lost}(t) \tag{23}$$

where, $T(t+\delta t)$ is acquired from Eq. 22, $T_{lost}(t)$ denotes the decreasing temperature by the heat transferring, which is defined as:

$$T_{lost}(t) = \frac{k}{k_s}\frac{\delta_x}{\pi r_a^2}\sum_{i=0}^{q-1}(g_i(\mathbf{x},t) - g_{i'}(\mathbf{x}+\mathbf{e}_i,t)) \tag{24}$$

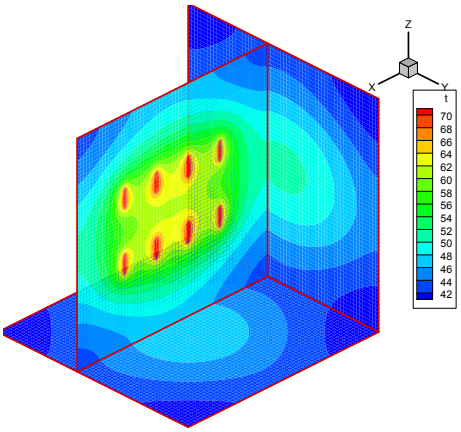

(a) Y-section($y = 25mm$)

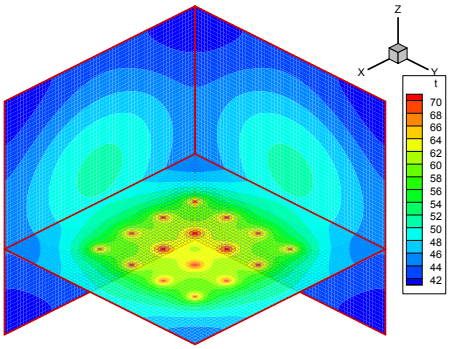

(b) Z-section($z = 23mm$)

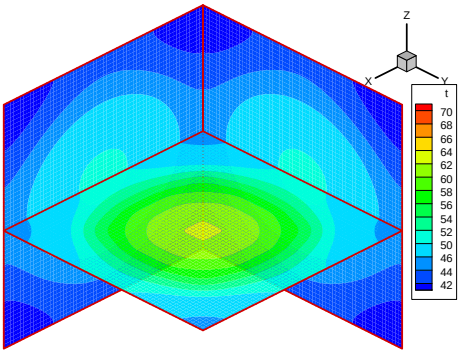

(c) Z-section($z = 30mm$)

Figure 7: Temperature contours

where the first two terms at the right of the equation is the coefficients.

After simulation, the temperatures at any places of the phantom would be known. Fig. 7 illustrates the temperature contours from three perpendicular sections. Also, the temperature at each point can be recorded. The temperatures where the thermocouples positioned, were analyzed by comparing with the experimental results. Fig. 8 shows the comparison. From the two comparing curves, we can find that the variation of the temperature obtained by the numerical method is almost similar to the experimental results. The comparison intensifies that the proposed model is effective and has enough accuracy.

The numerical method has been explained and verified in many studies(Chen and Doolen (1998)). The present calculation is mostly depended on the temperature variation model of the ferromagnetic seed. As long as the model is effective, the numerical results would be credible. However, the real status of the seed cannot be observed when they are in the phantom or in the body. The temperature variation of the seed in the phantom is different from that when directly imposed to the magnetic field. Although there have some empirical formulas, they can not be utilized directly. By using the numerical works, the model of temperature variation can be revised or improved. Then, the physical law of heat generation of the seed in tissue can be recognized.

5 Conclusion

This paper presents a numerical model to solve the heat transfer in magnetic induction hyperthermia. We demonstrate the procedures of solving the Pennes bio-heat equation by LBM. We treat the ferromagnetic seeds as the temperature boundary and develop the temperature model of the seed based on the Haider's method. We also implement several magnetic induction experiments to heat the phantom. Three phantoms having the same properties are used, each implanted with 32 seeds. Two thermocouples are placed to special positions to measure the temperature.

The comparisons between the experimental results and the numerical solutions show the proposed method has enough accuracy. It also indicates that the adopted temperature variation model is effective. The present work gives another numerical methods for bio-heat transfer problems. Except the ability of temperature prediction, the proposed method can be used to measure the clinical tumor temperature with the help of few thermometers. However, the parallel computing algorithm is expected, as LBM has the advantage of parallel computing.

Acknowledgement: The authors would like to thank Fuzhou Haolian Medical Technology Co., Ltd, which has provided some technical supports for the magnetic

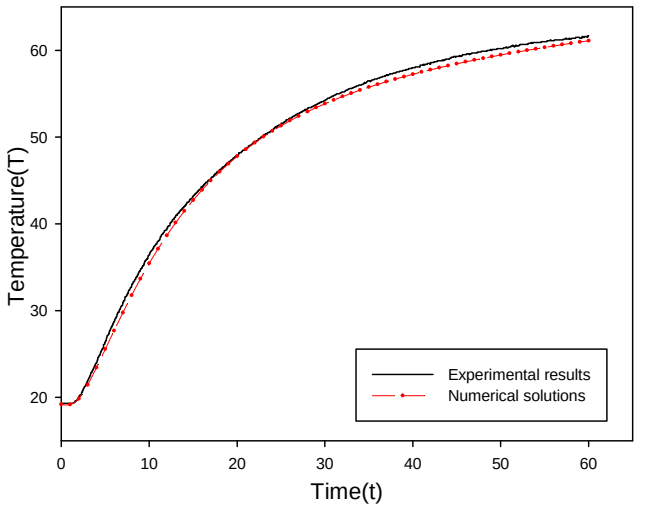

(a) Point 1

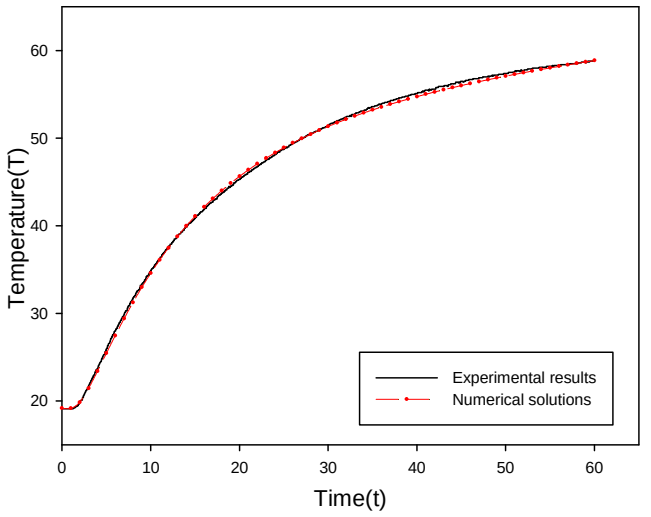

(b) Point 2

Figure 8: Comparison between the numerical and the experimental results

induction experiments.

References

Brezovich, I. A.; Lilly, M. B.; Meredith, R. F.; Weppelmann, B.; Henderson, R. A.; Brawner, W.; Salter, M. M. (1990): Hyperthermia of pet animal tumours with self-regulating ferromagnetic thermoseeds. *International Journal of Hyperthermia*, vol. 6, no. 1, pp. 117–130.

Chen, S.; Doolen, G. (1998): Lattice boltzmann method for fluid flows. *Annual Review of Fluid Mechanics*, vol. 30, no. 1, pp. 329–364.

Golneshan, A.; Lahonian, M. (2011): The effect of magnetic nanoparticle dispersion on temperature distribution in a spherical tissue in magnetic fluid hyperthermia using the lattice boltzmann method. *International Journal of Hyperthermia*, vol. 27, no. 3, pp. 266–274.

Guo, Z.; Zheng, C.; Shi, B. (2002): An extrapolation method for boundary conditions in lattice boltzmann method. *Physics of fluids*, vol. 14, pp. 2007.

Haider, S.; Cetas, T.; Wait, J.; Chen, J. (1991): Power absorption in ferromagnetic implants from radiofrequency magnetic fields and the problem of optimization. *Microwave Theory and Techniques, IEEE Transactions on*, vol. 39, no. 11, pp. 1817–1827.

He, X.; Chen, S.; Doolen, G. (1998): A novel thermal model for the lattice boltzmann method in incompressible limit. *Journal of Computational Physics*, vol. 146, no. 1, pp. 282–300.

Indik, J.; Indik, R.; Cetas, T. (1994): Fast and efficient computer modeling of ferromagnetic seed arrays of arbitrary orientation for hyperthermia treatment planning. *International Journal of Radiation Oncology* Biology* Physics*, vol. 30, no. 3, pp. 653–662.

Kotte, A.; Wieringen, N.; Lagendijk, J. (1998): Modelling tissue heating with ferromagnetic seeds. *Physics in medicine and biology*, vol. 43, pp. 105.

Latt, J.; Chopard, B.; Malaspinas, O.; Deville, M.; Michler, A. (2008): Straight velocity boundaries in the lattice boltzmann method. *Physical Review E*, vol. 77, no. 5, pp. 056703.

Murray, T. G.; Steeves, R. A.; Gentry, L.; Bresnick, G.; Boldt, H. C.; Mieler, W. F.; Tompkins, D. (1997): Ferromagnetic hyperthermia: Functional and histopathologic effects on normal rabbit ocular tissue. *International Journal of Hyperthermia*, vol. 13, no. 4, pp. 423–436.

Pennes, H. (1948): Analysis of tissue and arterial blood temperatures in the resting human forearm. *Journal of applied physiology*, vol. 1, no. 2, pp. 93–122.

Stauffer, P.; Cetas, T.; Fletcher, A.; Deyoung, D.; Dewhirst, M.; Oleson, J.; Roemer, R. (1984): Observations on the use of ferromagnetic implants for inducing hyperthermia. *Biomedical Engineering, IEEE Transactions on*, , no. 1, pp. 76–90.

Stauffer, P.; Cetas, T.; Jones, R. (1984): Magnetic induction heating of ferromagnetic implants for inducing localized hyperthermia in deep-seated tumors. *Biomedical Engineering, IEEE Transactions on*, , no. 2, pp. 235–251.

Steeves, R. A.; Murray, T. G.; Moros, E. G.; Boldt, H. C.; Mieler, W. F.; Paliwal, B. R. (1992): Concurrent ferromagnetic hyperthermia and 125i brachytherapy in a rabbit choroidal melanoma model. *International Journal of Hyperthermia*, vol. 8, no. 4, pp. 443–449.

Tompkins, D. T.; Partington, B. P.; Steeves, R. A.; Bartholow, S. D.; Paliwal, B. R. (1992): Effect of implant variables on temperatures achieved during ferromagnetic hyperthermia. *International Journal of Hyperthermia*, vol. 8, no. 2, pp. 241–251.